

UNVEILING SOURCES OF HEATING IN THE VICINITY OF THE ORION BN/KL HOT CORE AS TRACED BY HIGHLY EXCITED INVERSION TRANSITIONS OF AMMONIA

C. GODDI^{1,2}, L. J. GREENHILL², E. M. L. HUMPHREYS^{1,2}, C. J. CHANDLER³, AND L. D. MATTHEWS⁴

February 17, 2022

ABSTRACT

Using the Expanded Very Large Array, we have mapped the vicinity of the Orion BN/KL Hot Core with sub-arcsecond angular resolution in seven metastable inversion transitions of ammonia (NH₃): (J,K)=(6,6) to (12,12). This emission comes from levels up to 1500 K above the ground state, enabling identification of source(s) responsible for heating the region. We used this multi-transition dataset to produce images of the rotational/kinetic temperature ($T_{\text{rot}}/T_{\text{kin}}$) and the column density N_{col} of NH₃ for ortho and para species separately and on a position-by-position basis. We find T_{rot} and N_{col} in the range 160–490 K and $(1 - 4) \times 10^{17} \text{ cm}^{-2}$, respectively. Our spatially-resolved images show that the highest (column) density and hottest gas is found in a northeast-southwest elongated ridge to the southeast of Source I. We have also measured the ortho-para ratio of ammonia, estimated to vary in the range 0.9-1.6. Enhancement of ortho with respect to para and the offset of hot NH₃ emission peaks from known (proto)stellar sources provide evidence that the NH₃ molecules have been released from dust grains into the gas-phase through the passage of shocks and not by stellar radiation. We propose that the combined effect of Source I's proper motion and its low-velocity outflow impinging on a pre-existing dense medium is responsible for the excitation of NH₃ and the Orion Hot Core. Finally, we found for the first time evidence of a slow ($\sim 5 \text{ km s}^{-1}$) and compact ($\sim 1000 \text{ AU}$) outflow towards IRc7.

Subject headings: ISM: individual objects (Orion BN/KL) — ISM: molecules — ISM: abundances

1. INTRODUCTION

Orion BN/KL is the closest high-mass star forming region ($414 \pm 7 \text{ pc}$; Menten et al. 2007) and a compelling target for studying how massive young stellar objects (YSOs) form and interact with their surroundings. Objects of considerable long-term interest in BN/KL are the highly embedded radio Source I, believed to be a massive YSO (Reid et al. 2007; Matthews et al. 2010), and the Hot Core $>1''$ away, which is a rich source of molecular emission (e.g., Genzel & Stutzki 1989). In dust emission, the compact source SMA1 is visible $2''$ - $3''$ from Source I (Beuther et al. 2004), which also shows rich molecular emission (Beuther et al. 2005). On the other hand, only weak molecular thermal emission has been detected toward Source I (Beuther et al. 2005). However, its surrounding mass flows excite strong H₂O and SiO maser emission, permitting investigations of the 3-D gas dynamics at 10-1000 AU radii (Greenhill et al. 2004a; Matthews et al. 2010).

Despite intensive radio and infrared (IR) study, the primary heating sources for BN/KL ($\sim 10^5 L_{\odot}$) are still unknown. A strong mid-IR source, IRc2, has been long suspected to be the dominant energy source, but when observed at sub-arcsecond resolution, it breaks up into multiple peaks (Dougados et al. 1993; Greenhill et al. 2004b). Moreover, mid-IR observations have recently shown that IRc2 is not self-luminous, but is illuminated

and heated by Source I (Okumura et al. 2011). While it has been proposed that Source I is also (externally) heating the Hot Core (Hermesen et al. 1988), direct evidence is lacking and the kinetic temperature (T_{kin}) of molecular gas within $1''$ from Source I is not known. Tackling this uncertainty requires studies at radio rather than IR wavelengths, in order to penetrate the high column densities towards the Hot Core, and measurements of thermal rather than maser lines.

Ammonia (NH₃) is well suited to measuring T_{kin} over densities $> 10^4 \text{ cm}^{-3}$. In particular, metastable transitions ($J=K$) are interesting because they are collisionally excited, thus different (optically-thin) transitions can be used to determine T_{kin} via a rotational diagram analysis (Ho & Townes 1983). Inversion transitions from (J, K)=(8,8) to (14,14), with upper state energy levels ~ 800 - 2000 K above ground, have been previously detected toward BN/KL with the Effelsberg-100m telescope ($30''$ beam; Wilson et al. 1993), confirming the presence of hot molecular gas in the region but not localizing it. Wilson et al. (2000) mapped the Hot Core region in the (J, K)=(4,4) and (10,9) inversion transitions ($\sim 200 \text{ K}$ and $\sim 1350 \text{ K}$ above ground, respectively) with $\gtrsim 1''$ resolution. (10,9) is a nonmetastable transition of ortho-NH₃ and (4,4) is a metastable transition of para-NH₃, hence the Boltzmann analysis required assuming an ortho-para ratio, preventing an accurate measurement of T_{kin} .

In this Letter, we present new observations of (metastable) high- J inversion lines of NH₃ in Orion BN/KL. Using the Expanded Very Large Array (EVLA; Perley et al. 2011), we imaged at sub-arcsecond resolution seven NH₃ lines with energy levels high above the ground state (equivalent to 400-1600 K), from

cgoddi@eso.org

¹ European Southern Observatory, Karl-Schwarzschild-Strasse 2, D-85748 Garching bei München

² Harvard-Smithsonian Center for Astrophysics, 60 Garden Street, Cambridge, MA 02138

³ National Radio Astronomy Observatory, P.O. Box O, Socorro, NM 87801

⁴ MIT Haystack Observatory, Westford, MA 01886

$(J, K)=(6,6)$ to $(12,12)$. The multi-transition measurements enabled estimation of the temperature, density, and velocity field of (hot) molecular gas and hint at a possible excitation mechanism of the Hot Core.

2. OBSERVATIONS AND DATA REDUCTION

Observations of NH_3 were conducted using the EVLA of the National Radio Astronomy Observatory (NRAO). By using the (new) broadband EVLA K- and Ka-band receivers, we observed a total of seven metastable inversion transitions of NH_3 , from $(J, K)=(6,6)$ to $(12,12)$ at 1.3 cm (25–31 GHz). Transitions from $(6,6)$ to $(11,11)$ were observed separately in 3h tracks on several dates using the C configuration. The $(12,12)$ dataset was acquired in the hybrid CnB configuration. Table 1 summarizes the observations. Each transition was observed using a 4 MHz bandwidth ($\sim 40 \text{ km s}^{-1}$ at 30 GHz) consisting of 256 channels with a separation of 15.6 kHz. Typical on-source integration was 1.5h. Each transition was observed with “fast switching”, where 80s scans on-target were alternated with 40s scans of the nearby (1.3°) QSO J0541–0541 (measured flux density $\sim 0.7 \text{ Jy}$). We derived absolute flux calibration from observations of 3C 48 ($F_\nu = 1.1 \text{ Jy}$) or 3C 147 ($F_\nu = 1.4\text{--}1.6 \text{ Jy}$), depending on the epoch, and bandpass calibration from observations of 3C 84.

Using the Astronomical Image Processing System (AIPS) task IMAGR, we imaged the BN/KL region with cell size $0''.1$, covering a $50''$ field. We fitted and removed continuum emission from spectral cubes using AIPS’ IM-LIN. The data were processed both with and without velocity-smoothing, resulting in velocity resolutions of $0.15\text{--}0.19 \text{ km s}^{-1}$ and $0.6\text{--}0.8 \text{ km s}^{-1}$, respectively (depending on transition). The following analysis is based on the smoothed dataset. To match the angular resolution of different configurations, we produced maps setting the “ROBUST” weighting parameter to $\mathcal{R}=0$ for the transitions observed with the C-array and to $\mathcal{R}=5$ (natural weighting) for the $(12,12)$ transition observed with the CnB-array. We restored all images with a beam of size $0''.85 \times 0''.7$ (P.A.=0), approximately the average size among different transitions (see Table 1). After smoothing, the RMS noise per channel was typically $\sim 1.6 \text{ mJy beam}^{-1}$. The $(8,8)$ transition falls at the band-edge of the Ka-band receiver where performance was not optimal, resulting in lower-quality data compared with the other transitions. Hence, we excluded it from the following analysis. Moreover, inspection of data in post-processing revealed a 30% offset in the absolute flux scale for the $(9,9)$ dataset, possibly due to instability of the Ka-band system during the observations. We accounted for the systematic error by scaling the flux density by 30% in the final image of the $(9,9)$ transition.

3. RESULTS

For the first time we have mapped and localized the hot NH_3 gas from metastable transitions $(6,6)$ up to $(12,12)$ with sub-arcsecond resolution towards BN/KL. We observed three ortho $(6,6; 9,9; 12,12)$ and three para $(7,7; 10,10; 11,11)$ transitions so as to bracket an upper-state energy of 1000 K without exceeding 2000 K.

For each transition, we produced spectra by mapping each spectral channel and summing the flux density in each channel map (Figure 1). Multiple transitions show

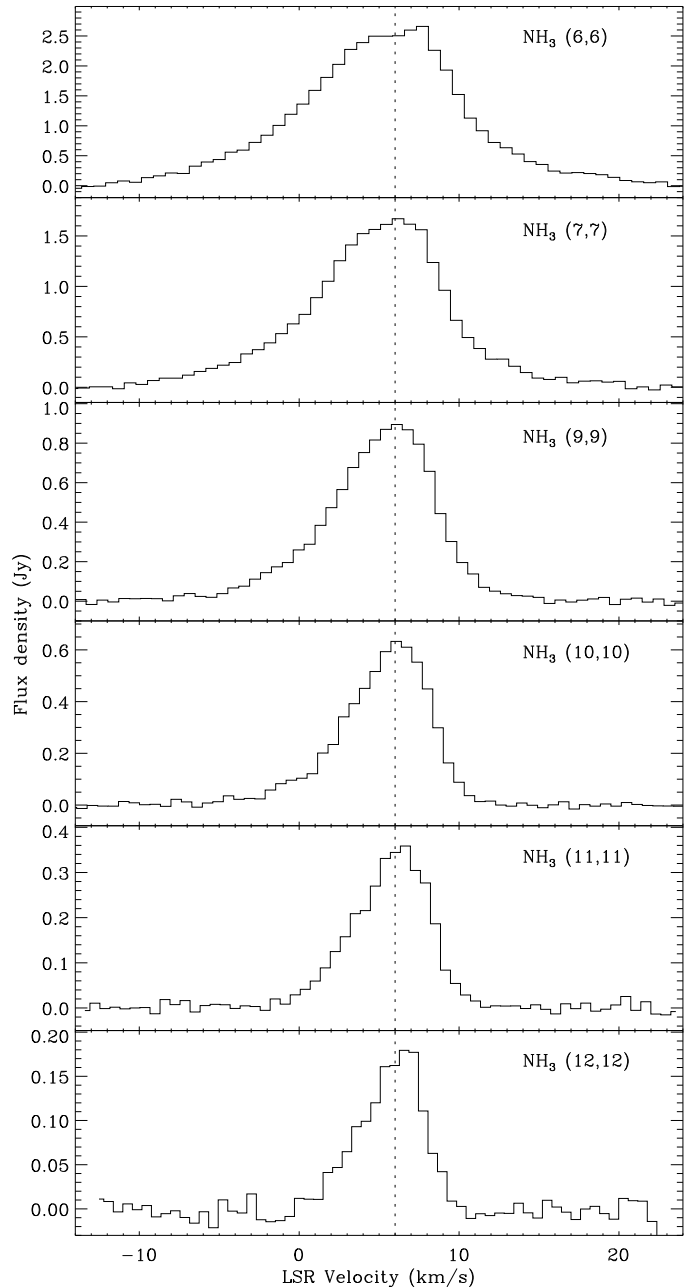


Figure 1. Spectra of various NH_3 inversion transitions observed toward Orion BN/KL with the EVLA. The velocity resolution is 0.7 km s^{-1} . The flux density is integrated over the Hot Core region and the radial velocities are with respect to the local standard rest (LSR). The vertical dashed line indicates a velocity of 6 km s^{-1} . Note that different flux density scales are adopted for different transitions.

similar line profiles and central velocities ($\sim 5\text{--}6 \text{ km s}^{-1}$), while velocity widths, σ_v , systematically decrease from $(6,6) \sim 5 \text{ km s}^{-1}$ to $(12,12) \sim 2 \text{ km s}^{-1}$, as determined from single-Gaussian fits (Table 1). By comparing with spectral profiles from the Effelsberg-100m telescope (assuming an equivalence relation $K=0.86 \text{ Jy}$; Wilson et al. 1993), most of the single-dish flux density for transitions from $(9,9)$ to $(12,12)$ was recovered by the EVLA. This

Table 1
Parameters of Observations.

Transition ^a (J,K)	ν_{rest} (MHz)	E_u/k ^b (K)	Date (yyyy/mm/dd)	EVLA Receiver	Synthesized Beam $\theta_M'' \times \theta_m''$	RMS ^c (mJy/beam)	F_{peak} ^d (Jy)	F_{int} (Jy km/s)	V_c (km/s)	σ_v (km/s)
(6,6)	25056.03	408	2010/10/11	K	0.93×0.76	3.3	2.54	30.78	5.31	4.85
(7,7)	25715.18	539	2010/10/12	K	0.91×0.72	3.3	1.62	16.25	5.14	4.01
(8,8)	26518.91	687	2010/12/17	Ka	0.91×0.79	18.	1.30	10.41	4.21	3.21
(9,9)	27477.94	853	2010/12/21	Ka	0.82×0.66	3.1	0.88	6.89	5.37	3.15
(10,10)	28604.74	1036	2010/12/29	Ka	0.84×0.65	3.0	0.61	3.89	5.68	2.54
(11,11)	29914.49	1238	2011/01/10	Ka	0.77×0.65	2.9	0.34	1.98	5.90	2.31
(12,12)	31424.94	1456	2011/02/05	Ka	0.77×0.63	3.5	0.17	0.82	5.93	1.91

Note. —

^a— Transitions include ortho-NH₃ ($K = 3n$) and para-NH₃ ($K \neq 3n$).

^b— Energy above the ground from the JPL database.

^c— RMS noise in a $\sim 0.2 \text{ km s}^{-1}$ channel (no velocity-smoothing).

^d— F_{peak} , F_{int} , V_c , and σ are estimated from single-Gaussian fits to the spectral profiles in Figure 1.

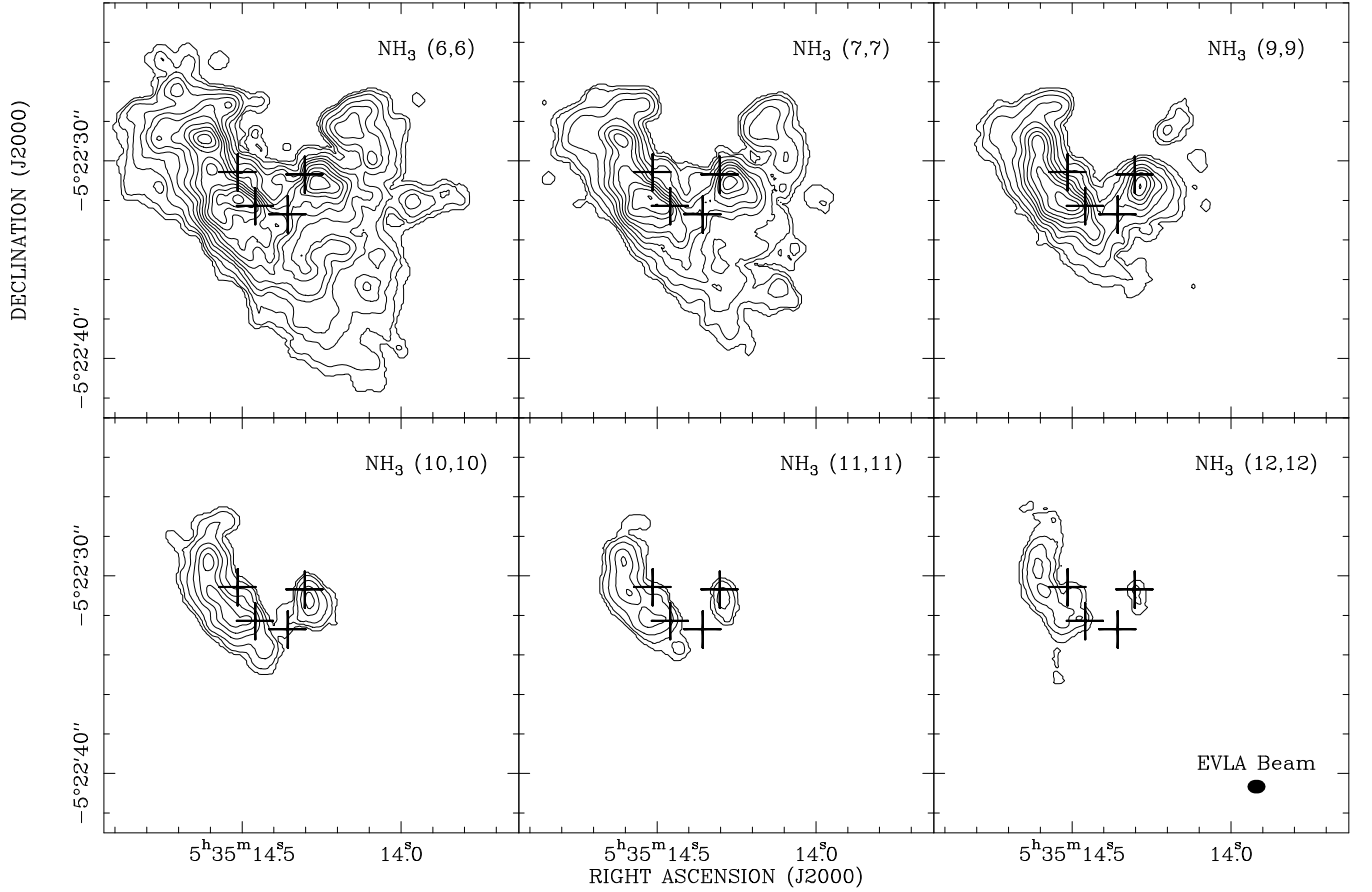


Figure 2. Total intensity images of NH₃ inversion transitions from (6,6) to (12,12) as observed toward Orion BN/KL with the EVLA. The images were integrated over the velocity range -14 km s^{-1} to 24 km s^{-1} with a flux cutoff of 5 mJy beam^{-1} ($\sim 3\sigma$) for all transitions. Contours are 1, 20, 50, ..., 550 (by 50) $\text{mJy beam}^{-1} \text{ km s}^{-1}$. The beam ($0''.85 \times 0''.7$) is shown in the right-lower corner. In every panel, the crosses mark the position of 4 YSOs in the region: sources I, SMA1, *n*, and IRC7 (left to right).

is not surprising considering that these transitions arise from levels $>850 \text{ K}$ above the ground, and are thus expected to arise from compact regions close to the exciting source.

We produced total intensity images of various NH₃ inversion transitions, integrated over the whole band (Fig. 2). In the image we included also the positions of the four YSOs Source I, *n*, SMA1, and IRC7. The low-excitation NH₃ emission (6,6; 7,7) is extended over

$\sim 15'' \times 15''$ ($0.03 \times 0.03 \text{ pc}$) and shows the typical Hot Core “heart-shaped” structure previously observed in various molecular lines: C₂H₅CN, CH₃OH, OCS (Friedel & Snyder 2008), CH₃CN (Zapata et al. 2011b), and NH₃ (4,4) (Wilson et al. 2000). The northwest (NW) lobe has the weakest integrated emission and it is not detected in the higher-*J* transitions, whose emission originates from the northeast lobe of the heart-shaped structure. This confirms earlier results from

Wilson et al. (2000) based on a comparison between (4,4) and (10,9). Interestingly, the highly-excited NH_3 line emission shows an “arc-like” ridge, oriented northeast-southwest (NE-SW), $\lesssim 3000$ AU long and $\lesssim 1000$ AU across, curving around Source I. Source I lies at the NW edge, indicating a lower column density towards its position.

West of Source I, we find high- J emission associated with IRC7. The structure of this emission in the transitions from (10,10) to (12,12) is bipolar and elongated north-south (N-S), with size ~ 1000 AU.

3.1. Temperature/density analysis

We estimated rotational temperature, T_{rot} , and column density, N_{col} , from rotational energy diagrams, using six observed transitions. We assumed that the inversion transitions are thermalized and optically thin. The beam-averaged N_{col} from an optically thin transition is given by (Friedel & Snyder 2008):

$$\frac{N_{\text{col}}}{Q} e^{-E_u/T_{\text{rot}}} = \frac{2.04W}{\theta_M \theta_m S \mu^2 \nu^3} \times 10^{20} \text{ cm}^{-2} \quad (1)$$

where Q is the partition function, E_u is the upper state energy of the transition (K), W is the integrated line intensity ($\text{Jy beam}^{-1} \text{ km s}^{-1}$), θ_M and θ_m are the FWHM Gaussian synthesized beam dimensions (arcseconds), $S \mu^2$ is the product of the line strength and the square of the molecular dipole moment (Debye^2), and ν is the transition frequency (GHz). For H_2 densities in the Hot Core ($\sim 10^7 \text{ cm}^{-3}$; Genzel & Stutzki 1989) we assume $T_{\text{rot}} = T_{\text{kin}}$ (Wilson et al. 2000), so in the following we simply refer to T_{kin} .

We performed separate temperature analyses for ortho and para species, enabling empirical determination of the NH_3 ortho-para ratio in the Hot Core: 0.9-1.6 ($\pm 0.05 - 0.1$) with an average over all pixels of 1.1. The highest values are located in the NW-side of the ridge which faces Source I.

We determined the distribution of T_{kin} and N_{col} on a position-by-position basis. We measured $T_{\text{kin}} \sim 160-490$ K ($\Delta T \lesssim 8$ K) and $N_{\text{col}} \sim (1-4) \times 10^{17} \text{ cm}^{-2}$ ($\Delta N \lesssim 10^{16} \text{ cm}^{-2}$), averaged on scales $\lesssim 1''$ (Fig. 3). The highest values of T_{kin} and N_{col} lie in a NE-SW elongated ridge offset (to the southeast) from Source I. At Source I’s position, we measure $T_{\text{kin}} \sim 260$ K and $N_{\text{col}} \sim 7 \times 10^{16} \text{ cm}^{-2}$. Temperature and density towards Source I are estimated using only ortho transitions because the signal-to-noise ratios in para data were insufficient. Consequently, total column density is probably 1.5-2 \times greater.

Wilson et al. (1993) reported 400 ± 40 K using the inversion lines (10,10) to (14,14) observed at $30''$ resolution, while Wilson et al. (2000) reported values in the range 130-170 K from $1''$ images of (4,4) and (10,9). In the paper presented here, high-excitation transitions observed at sub-arcsecond resolution enable us to map the gas density and temperature distribution with unprecedented precision. This has revealed hotter, denser material than previously derived from NH_3 measurements. The temperature inferred from high- J lines of CH_3CN is 200-600 K (Wang et al. 2010), consistent with our findings from NH_3 .

Our analysis assumes optically thin transitions (Wilson et al. 2000). Hyperfine-structure satellite lines

are outside of the bandwidths employed, hence direct estimation of optical depth is impossible. Hermsen et al. (1988) reported optical depths >1 for the (6,6) and (7,7) transitions. Non-negligible optical depths in the lowest available transitions (6,6 for ortho; 7,7 for para) might systematically boost the derived temperatures. We argue otherwise that this is not the case. Para-transitions yield higher temperatures than ortho-transitions, inconsistent with expectation of lower optical depth for (7,7) than (6,6). Moreover, rotation diagrams for individual pixels do not diverge from a linear trend for the lower (J,K) states.

3.2. Velocity field

The first moment maps of (6,6) and (7,7) in Figure 4 show that redshifted gas (7 to 14 km s^{-1}) is located on the NW part of the heart-shaped structure, blueshifted gas (-10 to 0 km s^{-1}) is concentrated towards the central part, while the NE lobe is around systemic velocity (0 to 7 km s^{-1}). The NH_3 emission shows a velocity gradient southward from Source I towards the Hot Core center, where the largest values of velocity dispersion are also observed. Unless we assume the presence of an additional embedded source in that location, this may indicate shock propagation in the Hot Core (see Sect. 4). Interestingly, we identified a N-S velocity gradient ($\Delta v \sim 5 \text{ km s}^{-1}$) in the bipolar structure traced by high- J NH_3 emission in IRC7, where line-widths also appears enhanced. The N-S bipolar morphology, the velocity gradient in the elongation axis, and the line-width enlargement provide strong evidence of a low-velocity outflow associated with IRC7.

4. DISCUSSION & CONCLUSIONS

Our multi-transition measurements of NH_3 emission enable the estimation of temperature and density of (hot) molecular gas at high-spatial resolution in the vicinity of Source I and the Hot Core. This complements the temperature distribution as a function of radius close to Source I inferred from radiative transfer modelling of SiO masing gas (Goddi et al. 2009). Maser action in the disk/wind from Source I implies temperatures 1000-2000 K inside ~ 100 AU and temperatures of 400-1000 K in the outflow at radii 100 AU to 1000 AU. A dust color temperature of ~ 700 K is consistent with this finding (Okumura et al. 2011). On the other hand, an NH_3 temperature of ~ 260 K toward Source I implies that hot NH_3 emission is not directly (radiatively-)excited by Source I. One explanation of this apparent discrepancy could be that a high ultraviolet radiation field in the vicinity of Source I may dissociate fragile molecules like NH_3 (dissociation energy 4 eV), while enhancing gas-phase abundance of SiO through grain sputtering. This would also explain the offset between Source I and the peak of high- J NH_3 emission.

What is exciting the high-energy transitions of NH_3 ? In fact, all known or suspected (massive) YSOs in the region are offset from peaks in hot NH_3 emission (Figure 2), and there is no evidence of any other embedded objects heating the Hot Core in the radio (Menten & Reid 1995), millimeter (Friedel & Snyder 2008), and infrared (Greenhill et al. 2004b). Additionally, the color temperature distribution from mid-IR measurements shows

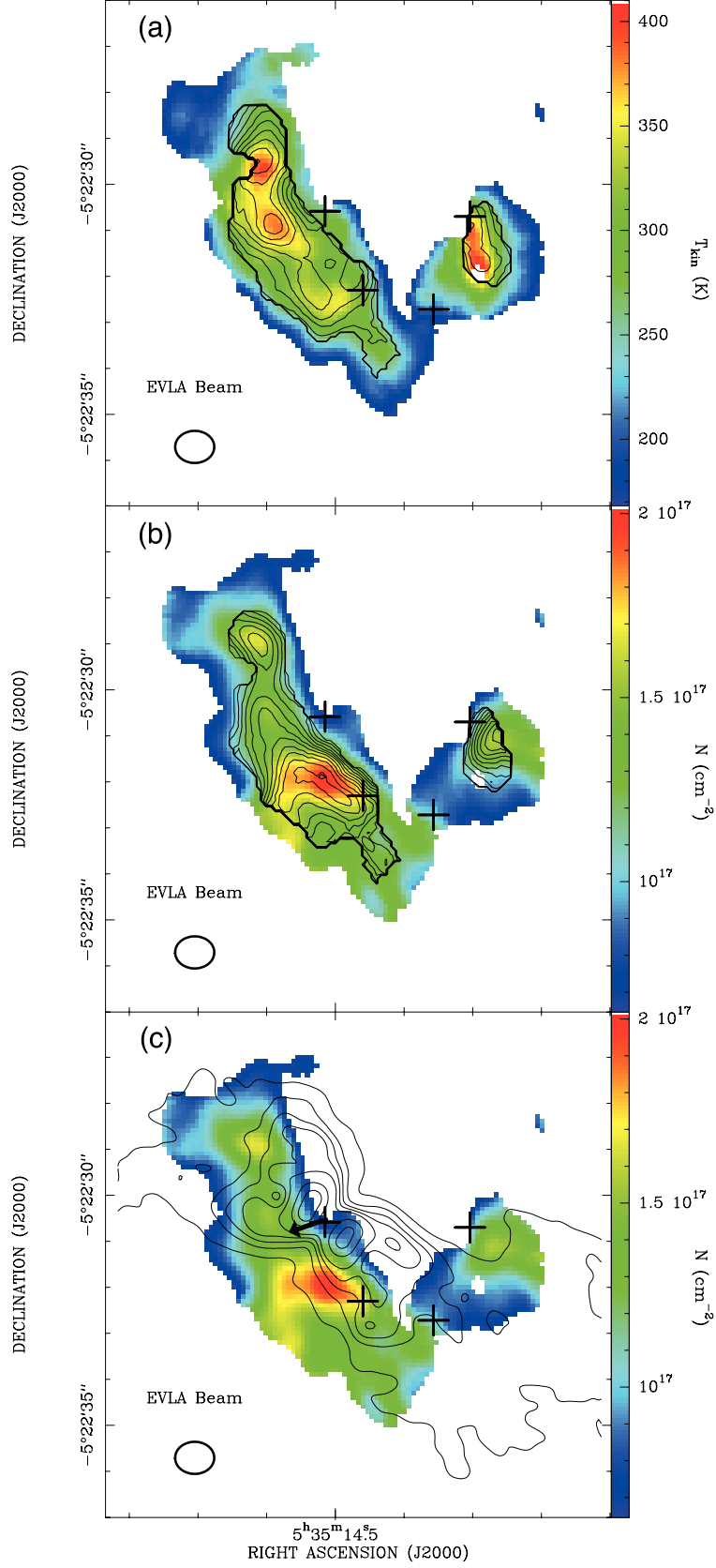


Figure 3. NH_3 rotational temperature (T_{rot}) and column density (N_{col}) maps of Orion BN/KL, obtained from ortho (colors) and para (contours in top two panels) inversion transitions. In all panels, the crosses mark the positions of sources I, SMA1, n, and IRC7 (left to right). (a) Map of T_{rot} averaged over LSR velocities -14 km s^{-1} to 24 km s^{-1} . Contour levels are 210 K to 480 K in increments of 30 K. Outside the region shown, the signal-to-noise ratio was insufficient to calculate T_{rot} ($\Delta T > 8 \text{ K}$) reliably. (b) Map of N_{col} obtained using equation 1. Contours are from 0.8 to $2 \times 10^{17} \text{ cm}^{-2}$ in increments of 10^{16} cm^{-2} ($\Delta N \lesssim 10^{16} \text{ cm}^{-2}$). Note that the densest and hottest NH_3 are found in a northeast-southwest elongated ridge to the southeast of Source I. (c) Ortho N_{col} (colors) with SiO $v=0, J=2-1$ total intensity (contours) from Plambeck et al. (2009) overplotted. Contours are 0.1, 0.3, 0.5, 0.7, 1, 2, 3 Jy beam $^{-1} \text{ km s}^{-1}$. The arrow indicates the proper motion of Source I in the Orion rest-frame (Goddi et al. 2011).

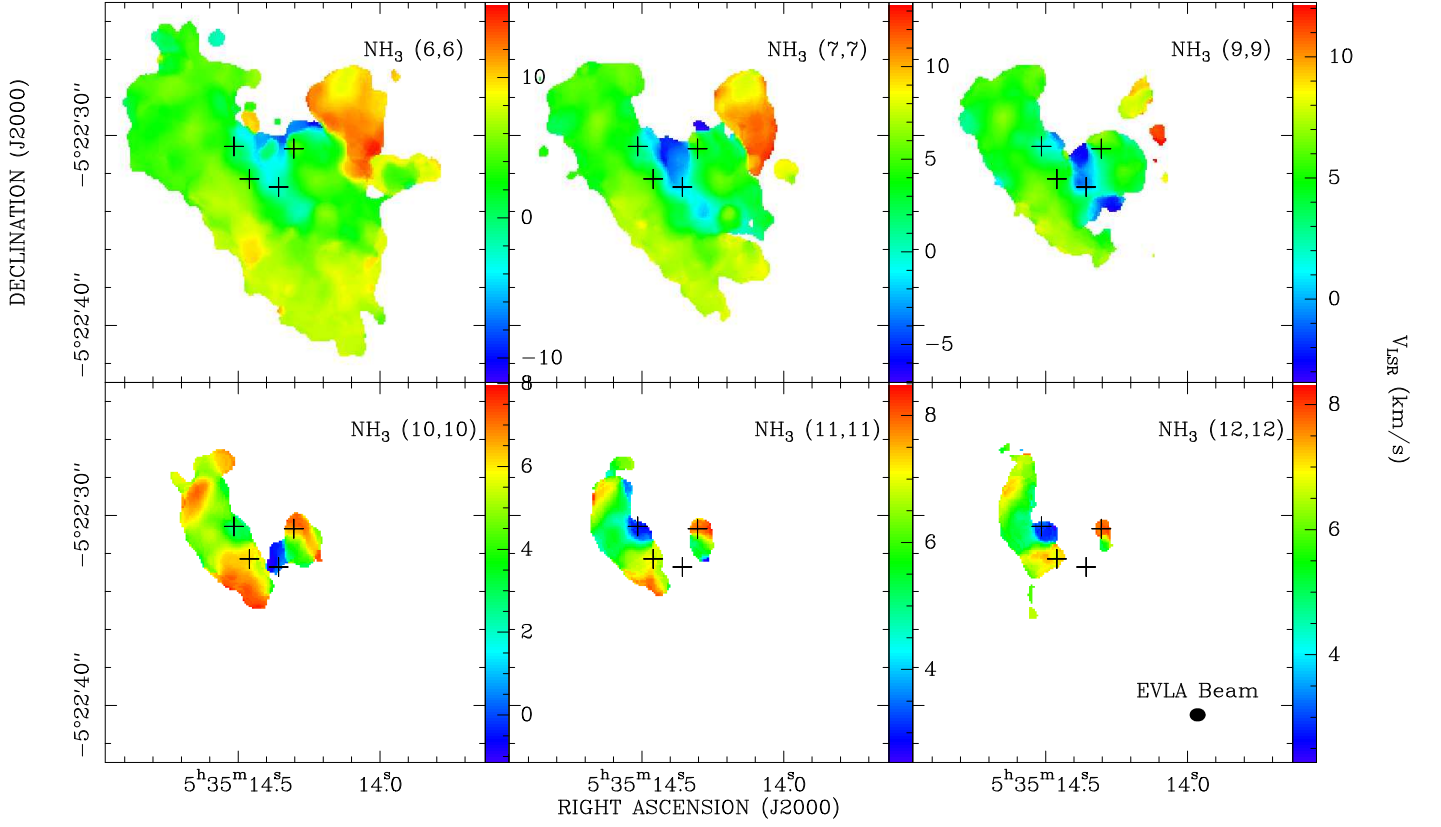


Figure 4. Velocity fields of NH_3 inversion transitions from (6,6) to (12,12). Colors indicate V_{LSR} in km s^{-1} . Color scales are compressed with increasing quantum number to clearly show velocity structure. In each panel, the crosses mark the position of sources I, SMA1, n , and IRc7 (from left to right). All transitions show a velocity gradient southward from Source I towards the Hot Core center (the less clear signature in the upper panels is due to the expanded color scale).

a decreasing gradient from Source I to the Hot Core (Okumura et al. 2011). We propose that the elevated gas temperatures measured from NH_3 in the Hot Core are produced by shock-waves and not by stellar radiation. Theoretical models suggest that NH_3 might form through surface chemistry on dust grains and then be released in the gas-phase by the passage of shocks, either through hydrodynamic gas-grain interaction (Flower & Pineau des Forets 1994; Flower et al. 1995) or shock-induced IR radiation (Taylor & Williams 1996). Indeed, enhanced NH_3 has been observed in the L1157 low-mass outflow (Tafalla & Bachiller 1995), as well as towards a dense (quiescent) clump downstream from the high-mass protostellar jet HH 80 North (Girart et al. 1998). Umemoto et al. (1999) report also ortho-para enhancement in the L1157 outflow. Several pieces of evidence corroborate the shock hypothesis in the Orion Hot Core: the offset of hot NH_3 emission peaks from known (proto)stellar sources, the high T_{kin} , the departure of the ortho-para ratio from the statistical equilibrium value (1.0; Umemoto et al. 1999), and the high abundances of shock tracer molecules (SiO , SO , SO_2) and common molecular constituents of interstellar ices ($\text{C}_2\text{H}_5\text{CN}$, CH_3OH , CH_3CN ; van Dishoeck & Blake 1998).

What generates the shocks? Recent studies report strong evidence that a dynamical interaction occurred ~ 500 years ago between Source I and the high-mass YSO BN (Gómez et al. 2008; Goddi et al. 2011). The stellar interaction resulted in high stellar proper motions for Source I and BN and possibly produced the fast bullet outflow traced by CO and H_2 (Zapata et al. 2009; Bally et al. 2011; Goddi et al. 2011). In this framework, it has recently been proposed that the Hot Core might have originated from the impact of a shock-wave onto a pre-existing dense core, driven by either the expansion of a dense bubble of material previously associated with BN and Source I (Zapata et al. 2011a) and/or the fast bullets (Zapata et al. 2011b). Data in Figure 3c, however, suggest another possibility. The relationship between the high column density gas as traced by NH_3 , the Source I proper motion, and the Source I outflow as traced by SiO emission (Plambeck et al. 2009) together suggest that the Source I outflow drives compression and shocks in the surrounding medium. The relative narrowness of the SW outflow in close proximity of the column density peak is suggestive of ram pressure effects caused by the outflow and the YSO proper motion. The more open NE lobe, its apparent symmetry about the flow axis, and its extension beyond the northern NH_3 clump may indicate that the outflow is in front of or behind the dense gas, compressing it more along the line of sight. Part of the mechanical energy of the outflow could be dissipated and contribute to gas heating. This is also consistent with the ortho-para ratio being larger in the NW-side of the ridge facing Source I.

Detailed modeling, including shock-physics as well as dust/gas-phase chemistry, will be required to discriminate between different (shock) scenarios proposed for the Hot Core excitation. However, the shock velocities implied by different scenarios and inferred NH_3 chemistry are suggestive. Flower & Pineau des Forets (1994) showed that shocks with velocities of $10\text{--}50\text{ km s}^{-1}$ (C-

type) efficiently sublimate ice mantles, ejecting volatile molecules intact and enabling efficient abundance enhancement. Shocks with velocities $<10\text{ km s}^{-1}$ would have just a diminished impact on grain-mantle evaporation and NH_3 abundance enhancement, which weighs against the hypothesized slowly-expanding bubble (7 km s^{-1})⁵ as the main mechanism for the Hot Core excitation. In contrast, fast bullets ($>100\text{ km s}^{-1}$) would drive strong J-type shocks, causing grain sputtering and molecular dissociation. Reformation of NH_3 by gas-phase chemistry is possible but less likely on the short dynamical time of the region (~ 500 years). Nonetheless, existing models have not investigated chemical evolution behind J-type shocks. Intermediate-velocity bullets traced by H_2 ($30\text{--}70\text{ km s}^{-1}$; Bally et al. 2011) could in principle drive C-type shocks and release NH_3 as well as excite H_2 emission, but the poor correlation between NH_3 and mid-IR/ H_2 emission (Shuping et al. 2004) argues against this possibility. We note that the impact of outflow from Source I (20 km s^{-1}) in combination with proper motion of 12 km s^{-1} could efficiently heat the Hot Core with limited molecular dissociation. Favre et al. (2011) reported an anticorrelation of methyl-formate and H_2 in the Hot Core and proposed a similar mechanism for its excitation. Extinction could however be responsible for the observed anticorrelation.

In summary, we suggest that local mechanical interaction of Source I with the Orion Hot Core is more likely to be responsible for enhanced NH_3 abundance and heating of gas in the Core than the consequence of the hypothesized explosive event tied to the protostellar dynamical interaction.

We thank Malcolm Walmsley and Steve Longmore for useful discussions, and the anonymous referee for a constructive report. These data were obtained under EVLA OSRO program 10B-225 and the work was supported by the National Science Foundation (AST 0507478).

REFERENCES

- Bally, J., et al. 2011, *ApJ*, 727, 113
- Beuther, H., et al. 2004, *ApJ*, 616, L31
- Beuther, H., et al. 2005, *ApJ*, 632, 355
- Dougados, C., Lena, P., Ridgway, S. T., Christou, J. C., & Probst, R. G. 1993, *ApJ*, 406, 112
- Favre, C., et al. 2011, *arXiv:1103.2548*
- Flower, D. R., & Pineau des Forets, G. 1994, *MNRAS*, 268, 724
- Flower, D. R., Pineau des Forets, G., & Walmsley, C. M. 1995, *A&A*, 294, 815
- Friedel, D. N., & Snyder, L. E. 2008, *ApJ*, 672, 962
- Genzel, R., & Stutzki, J. 1989, *ARA&A*, 27, 41
- Girart, J., Estalella, R., & Ho, P. T. P. 1998, *ApJ*, 495, L59
- Goddi, C., Greenhill, L. J., Chandler, C. J., Humphreys, E. M. L., Matthews, L. D., & Gray, M. D. 2009, *ApJ*, 698, 1165
- Goddi, C., Humphreys, E. M. L., Greenhill, L. J., Chandler, C. J., & Matthews, L. D. 2011, *ApJ*, 728, 15
- Gómez, L., Rodríguez, L. F., Loinard, L., Lizano, S., Allen, C., Poveda, A., & Menten, K. M. 2008, *ApJ*, 685, 333
- Greenhill, L. J., Reid, M. J., Chandler, C. J., Diamond, P. J., & Elitzur, M. 2004a, *Star Formation at high-angular Resolution*, 221, 155
- Greenhill, L. J., Gezari, D. Y., Danchi, W. C., Najita, J., Monnier, J. D., & Tuthill, P. G. 2004b, *ApJ*, 605, L57

⁵ The 15 km s^{-1} value quoted in Zapata et al. (2011a) is divided by two for spherical expansion.

- Hermesen, W., Wilson, T. L., Walmsley, C. M., & Henkel, C. 1988, A&A, 201, 285
- Ho, P. T. P., & Townes, C. H. 1983, ARA&A, 21, 239
- Matthews, L. D., Greenhill, L. J., Goddi, C., Chandler, C. J., Humphreys, E. M. L., & Kunz, M. W. 2010, ApJ, 708, 80
- Menten, K. M., & Reid, M. J. 1995, ApJ, 445, L157
- Menten, K. M., Reid, M. J., Forbrich, J., & Brunthaler, A. 2007, A&A, 474, 515
- Okumura, S.-i., Yamashita, T., Sako, S., Miyata, T., Honda, M., Kataza, H., & Okamoto, Y. K. 2011, arXiv:1104.4394
- Perley, R.A., Chandler, C.J., Butler, B.J., Wrobel, J.M. 2011, ApJ, in press
- Plambeck, R. L., et al. 2009, ApJ, 704, L25
- Reid, M. J., Menten, K. M., Greenhill, L. J., & Chandler, C. J. 2007, ApJ, 664, 950
- Shuping, R. Y., Morris, M., & Bally, J. 2004, AJ, 128, 363
- Tafalla, M., & Bachiller, R. 1995, ApJ, 443, L37
- Taylor, S. D., & Williams, D. A. 1996, MNRAS, 282, 1343
- Umemoto, T., Mikami, H., Yamamoto, S., & Hirano, N. 1999, ApJ, 525, L105
- van Dishoeck, E. F., & Blake, G. A. 1998, ARA&A, 36, 317
- Wang, K.-S., Kuan, Y.-J., Liu, S.-Y., & Charnley, S. B. 2010, ApJ, 713, 1192
- Wilson, T. L., Henkel, C., Huttemeister, S., Dahmen, G., Linhart, A., Lemme, C., & Schmid-Burgk, J. 1993, A&A, 276, L29
- Wilson, T. L., Gaume, R. A., Gensheimer, P., & Johnston, K. J. 2000, ApJ, 538, 665
- Zapata, L. A., Schmid-Burgk, J., Ho, P. T. P., Rodríguez, L. F., & Menten, K. M. 2009, ApJ, 704, L45
- Zapata, L. A., Loinard, L., Schmid-Burgk, J., Rodríguez, L. F., Ho, P. T. P., & Patel, N. A. 2011a, ApJ, 726, L12
- Zapata, L. A., Schmid-Burgk, J., & Menten, K. M. 2011b, A&A, 529, A24